

LASERS

https://doi.org/10.1070/QEL17305

Numerical simulation of the divergence and optical confinement factor of a semiconductor laser with an asymmetric periodic multilayer AlGaInAs/InP waveguide

V.D. Kurnosov, K.V. Kurnosov

Abstract. **The divergence and optical confinement factor of a semiconductor laser with an asymmetric periodic (multilayer) waveguide are numerically simulated. The reasons for the choice of the given heterostructure design are explained, and the consequences of choosing other layer structures are considered. It is shown how to choose the active waveguide thickness, the active region position on the waveguide, and the multilayer waveguide grating period.**

Keywords: *radiation divergence, optical confinement factor, multilayer waveguide, semiconductor laser.*

1. Introduction

High-power semiconductor lasers have found wide application in fibre-optic communication lines, medicine, environmental monitoring systems, spectroscopy of industrial gases, etc. It is known that radiation in the spectral range of 1.5–1.6 μm is eye-safe.

The parameters of high-power semiconductor lasers in the $In_{1-x-y}Ga_yAl_xAs/InP$ system emitting at 1.5–1.6 μm were studied in [1, 2]. The parameters of a laser with a cavity length of 1.6 mm and a mesa-stripe contact width of 3 μm were investigated in work [1], while a laser with a cavity length of 2.6 mm and a mesa-stripe width of 100 μm was examined in [2]. The lasers in both cases were fabricated from one and the same heterostructure (HS). The calculated optical confinement factor was 0.0132. However, the high laser beam divergence in the plane perpendicular to the p–n junction, which is ~45° at half maximum, does not allow one to effectively use these lasers in optical systems and efficiently couple their radiation into optical fibres.

Today, the most popular approach for decreasing the laser beam divergence [3–5] is based on the use of a periodic multilayer waveguide with irregular periodicity, which makes it possible to obtain laser radiation with a low beam divergence in the plane perpendicular to the p–n junction. Unfortunately, the mentioned works present only the investigation results and do not explain the reasons for the choice of the heterostructure design used for the laser.

In the present work, we try to prove the choice of the thicknesses of laser layers used in [6] and to explain the results of the choice of other combinations of layer thicknesses in a multilayer waveguide. The main goal of our simulation was to decrease the laser beam divergence in the plane perpendicular to the p–n junction from 45° to 35° with retaining (or increasing) the optical confinement factor obtained in [1, 2].

We considered the heterostructure used in [1, 2], which was improved taking into account the HS design from [3–5]. The HS used in [1, 2] contained two quantum wells, each of them 0.007 μm thick, and was sandwiched between waveguide layers with thicknesses of 0.01 and 0.73 μm. To simplify calculations in the present work, we used, instead of two 0.007-μm quantum wells, one quantum well with a double thickness (0.014 μm), which was sandwiched between waveguide layers with thicknesses L_2 and L_1, and a periodic (multilayer) optically coupled waveguide. Figure 1 shows the refractive index distribution in the one-dimensional structure used for numerical simulation of the laser.

The refractive indices of the layers of the multilayer waveguide in the $In_{1-x-y}Ga_yAl_xAs/InP$ system were determined by formulae given in [7]. It was assumed that absorption in these layers is absent. The L_2, L_{ac}, and L_1 layers form a waveguide with the active region (AR), whose refractive index n_{ac} is higher than n_{b1}, n_{b2} and higher than n_1, n_2. Changes in refractive index n_{ac} due injection of carries into the AR were also ignored. The thickness of the active part of the multilayer waveguide is $L_w = L_2 + L_{ac} + L_1$ (in [3–5], this layer is called defect layer).

Below, we will show that the use of the HS parameters recommended in [6] for our calculations led to a good coincidence between the theoretically calculated and experimental radiation divergences.

2. Relations for calculating the parameters of a one-dimensional multilayer waveguide

The numerical simulation of a multilayer waveguide was performed taking into account the results obtained in [8–11].

Let us write the expressions for the electric field in each homogeneous layer of a multilayer waveguide in the form

$$E_s(x) = E_{00}\exp[h_s(x+L)], \quad x \leqslant -L, \tag{1}$$

$$E_1(x) = E_{10}\cos(h_1x - \alpha_1), \quad -L \leqslant x \leqslant -(L_{ac} + L_1 + a), \tag{2}$$

$$E_2(x) = E_{20}\cos(h_2x - \alpha_2), \quad -(L_{ac} + L_1 + a) \leqslant x \leqslant -(L_1 + a), \tag{3}$$

$$E_3(x) = E_{30}\cos(h_3x - \alpha_3), \quad -(L_1 + a) \leqslant x \leqslant -a, \tag{4}$$

$$E_{a_{n-1}}(x,n) = a_{n-1}\exp\{-ik_1[x - (n-1)\Lambda]\} + b_{n-1}$$

$$\times \exp\{ik_1[x - (n-1)\Lambda]\}, \quad (n-2)\Lambda + b \leqslant x \leqslant (n-1)\Lambda, \tag{5}$$

V.D. Kurnosov, K.V. Kurnosov Open Joint-Stock Company M.F. Stel'makh Polyus Research Institute, ul. Vvedenskogo 3, korp. 1, 117342 Moscow, Russia; e-mail: webeks@mail.ru

Received 25 February 2020; revision received 19 April 2020
Kvantovaya Elektronika **50** (9) 816–821 (2020)
Translated by M.N. Basieva

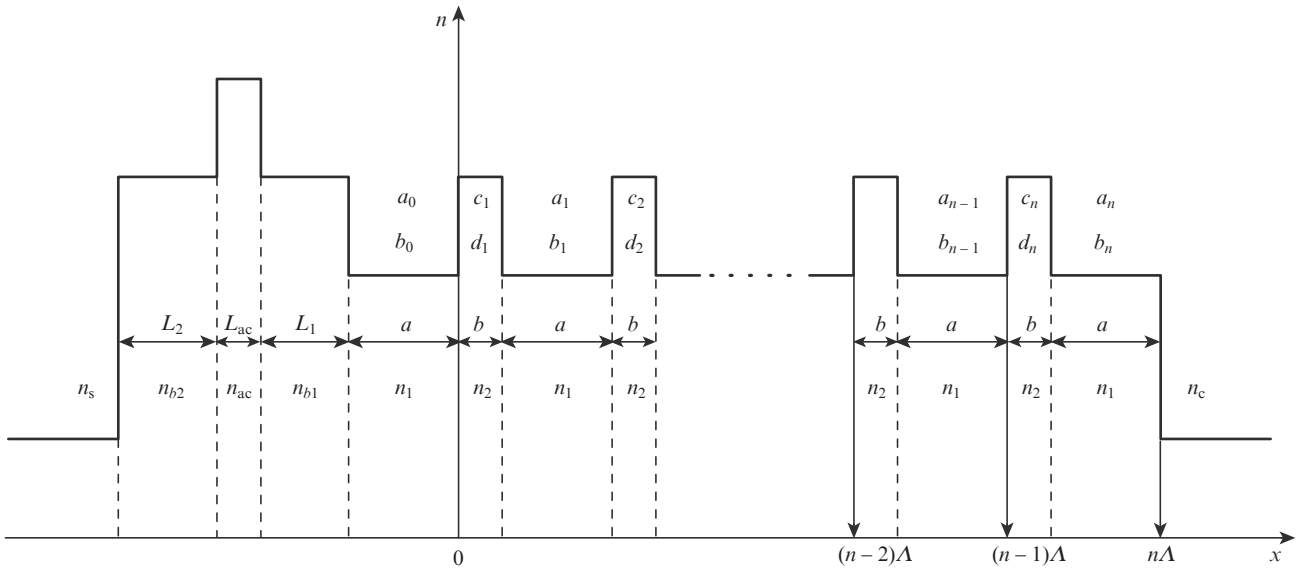

Figure 1. Schematic of the heterostructure of a semiconductor laser with an asymmetric periodic multilayer waveguide. L_{ac} is the thickness of the laser AR; a and b are the thicknesses of the multilayer waveguide layers; n_{b1}, n_{ac}, n_{b2}, n_1, and n_2 are the refractive indices of the corresponding layers; and n_s and n_c are the refractive indices of the substrate and cladding, respectively.

$$E_{c_n}(x,n) = c_n \exp\{-ik_2[x-(n-1)\Lambda]\} + d_n$$

$$\times \exp\{ik_2[x-(n-1)\Lambda]\},\ (n-1)\Lambda \leqslant x \leqslant (n-1)\Lambda + b, \quad (6)$$

$$E_{a_n}(x,n) = a_n \exp[-ik_1(x-n\Lambda)]$$

$$+ b_n \exp[ik_1(x-n\Lambda)],\ (n-1)\Lambda + b \leqslant x \leqslant n\Lambda, \quad (7)$$

$$E_4(x) = E_{40}\exp[h_c(n\Lambda - x)],\quad x \geqslant n\Lambda, \quad (8)$$

where

$$h_s = k_0\sqrt{\beta^2 - n_s^2};\ h_1 = k_0\sqrt{n_{b2}^2 - \beta^2};\ h_2 = k_0\sqrt{n_a^2 - \beta^2};$$

$$h_3 = k_0\sqrt{n_{b1}^2 - \beta^2};\ k_1 = k_0\sqrt{n_1^2 - \beta^2};\ k_2 = k_0\sqrt{n_2^2 - \beta^2};$$

$$h_c = k_0\sqrt{\beta^2 - n_c^2};\quad L = L_2 + L_{ac} + L_1 + a;$$

$k_0 = 2\pi/\lambda_0$ is the wave vector of radiation in vacuum; $\Lambda = a + b$ is the grating period; $\lambda_0 = 1.55$ μm; h_s, h_i, h_c, k_1, and k_2 ($i = 1-3$) are the propagation constants of plane waves in the direction of the x axis; and β is the effective refractive index in the direction of the z axis. The electric field distribution inside each homogeneous layer of the nth waveguide cell is represented in the form of the sum of the incident and reflected plane waves with amplitudes a_n, b_n and c_n, d_n in a and b layers, respectively [8–10].

Matching expressions for the electric field and its derivative at points $x = -(L_2 + L_{ac} + L_1 + a)$, $x = -(L_{ac} + L_1 + a)$, and $x = -(L_1 + a)$, we obtain [11]

$$\alpha_1 = -h_1 L + \arctan\left(\frac{h_s}{h_1}\right),$$

$$\alpha_2 = -h_2(L_1 + L_{ac} + a) + \arctan\left\{\frac{h_1}{h_2}\tan[h_1(L_1 + L_{ac} + a) + \alpha_1]\right\},$$

$$\alpha_3 = -h_3(L_1 + a) + \arctan\left\{\frac{h_2}{h_3}\tan[h_2(L_1 + a) + \alpha_2]\right\}.$$

Doing the same at point $x = -a$, we have

$$a_0 = \frac{1}{2}E_{30}\exp(-ik_1 a)\left[\cos(h_3 a + \alpha_3) - \frac{h_3}{ik_1}\sin(h_3 a + \alpha_3)\right],$$

$$b_0 = \frac{1}{2}E_{30}\exp(ik_1 a)\left[\cos(h_3 a + \alpha_3) + \frac{h_3}{ik_1}\sin(h_3 a + \alpha_3)\right].$$

Repeating this procedure at point $x = (n-1)\Lambda$, we find

$$c_n = \frac{1}{2}\left[a_{n-1}\left(1 + \frac{k_1}{k_2}\right) + b_{n-1}\left(1 - \frac{k_1}{k_2}\right)\right],$$

$$d_n = \frac{1}{2}\left[a_{n-1}\left(1 - \frac{k_1}{k_2}\right) + b_{n-1}\left(1 + \frac{k_1}{k_2}\right)\right].$$

Taking into account Eqn (9) from work [8] leads to

$$a_{n-1} = Aa_n + Bb_n,\quad b_{n-1} = Ca_n + Db_n.$$

Taking into account Eqns (20) and (30)–(32) from [8], we obtain

$$a_N = a_0(DU_{N-1} - U_{N-2}) - b_0 BU_{N-1},$$

$$b_N = -a_0 CU_{N-1} + b_0(AU_{N-1} - U_{N-2}),$$

where

$$U_{N-1} = \frac{\sin(NK\Lambda)}{\sin(K\Lambda)};\ U_{N-2} = \frac{\sin[(N-1)K\Lambda]}{\sin(K\Lambda)};$$

$$K = \frac{1}{\Lambda}\arccos\left(\frac{A+D}{2}\right)$$

is the Bloch wave function, n is the layer number, and N is the number of layers.

Matching function $E_{a_n}(x, n)$ and its derivative with $E_4(x)$ at point $x = n\Lambda$, we come to the following dispersion equation, which makes it possible to find β:

$$y(\beta) = AU_{N-1} - U_{N-2} - \frac{a_0}{b_0}CU_{N-1} + \frac{h_c - ik_1}{h_c + ik_1} \times\left[\frac{a_0}{b_0}(DU_{N-1} - U_{N-2}) - BU_{N-1}\right], \quad (9)$$

where

$$A = \exp(ik_1a)\left[\cos(k_2b) + \frac{i}{2}\left(\frac{k_1}{k_2} + \frac{k_2}{k_1}\right)\sin(k_2b)\right];$$

$$B = \exp(-ik_1a)\frac{i}{2}\left(\frac{k_2}{k_1} - \frac{k_1}{k_2}\right)\sin(k_2b);$$

$$C = \exp(ik_1a)\frac{-i}{2}\left(\frac{k_2}{k_1} - \frac{k_1}{k_2}\right)\sin(k_2b);$$

$$D = \exp(-ik_1a)\left[\cos(k_2b) - \frac{i}{2}\left(\frac{k_1}{k_2} + \frac{k_2}{k_1}\right)\sin(k_2b)\right].$$

There is a number of works (for example, [12, 13]) devoted to the analysis and search for zeros of functions similar to (9). We will follow work [13]. Let us plot the graph of function (9) similar to that given in [13] and find the value of β corresponding to the zero- and first-order modes. We will restrict ourselves to consideration of these modes. Calculations show that higher-order modes can be neglected because their optical confinement factors are lower than that of the zero and first modes [5]. It is also follows from calculations that the values of β for the chosen refractive indices of the multilayer waveguide satisfy the condition for the existence of waveguide modes and the absence of mode leakage into the substrate and cladding [14].

The optical confinement factor was determined as the intensity ratio [15]

$$\Gamma_{ac} = \frac{I_2}{I_s + I_1 + I_2 + I_3 + I_c + I_a + I_4} = I_2, \quad (10)$$

where $I_s+I_1+I_2+I_3+I_c+I_a+I_4=1$ (normalisation condition); $N = 7$;

$$I_s = \int_{-\infty}^{-L} E_s(x)^2 dx;\ I_1 = \int_{-L}^{-(L_{ac}+L_1+a)} E_1(x)^2 dx;$$

$$I_2 = \int_{-(L_{ac}+L_1+a)}^{-(L_1+a)} E_2(x)^2 dx;\ I_3 = \int_{-(L_1+a)}^{-a} E_3(x)^2 dx;$$

$$I_c = \sum_{n=1}^{7}\int_{(n-1)\Lambda}^{(n-1)\Lambda+b} E_{c_n}(x,n)^2 dx;$$

$$I_a = \sum_{n=0}^{7}\int_{(n-1)\Lambda+b}^{n\Lambda} E_{a_n}(x,n)^2 dx;$$

$$I_4 = \int_{n\Lambda}^{\infty} E_4(x)^2 dx.$$

The experimental far-field radiation pattern is characterised by the beam divergence determined as the total angle measured at half maximum of intensity. In the far-field zone, the intensity ratio of radiation propagating in the direction of angle θ to radiation propagating in the zero angle direction is [16]

$$Z(\theta) = I(\theta)/I(0) = \frac{\cos^2\theta\,|U_s(\theta)+U_1(\theta)+U_2(\theta)+U_3(\theta)+U_c(\theta)+U_a(\theta)+U_4(\theta)|^2}{|U_s(0)+U_1(0)+U_2(0)+U_3(0)+U_c(0)+U_a(0)+U_4(0)|^2}, \quad (11)$$

where

$$U_s(\theta)=\int_{-\infty}^{-L} E_s(x)\xi(x,\theta)dx;\ U_1(\theta)=\int_{-L}^{-(L_{ac}+L_1+a)} E_0(x)\xi(x,\theta)dx;$$

$$U_2(\theta)=\int_{-(L_{ac}+L_1+a)}^{-(L_1+a)} E_2(x)\xi(x,\theta)dx;$$

$$U_3(\theta)=\int_{-(L_1+a)}^{-a} E_3(x)\xi(x,\theta)dx;$$

$$U_c(\theta)=\sum_{n=1}^{7}\int_{(n-1)\Lambda}^{(n-1)\Lambda+b} E_{c_n}(x,n)\ \xi(x,\theta)dx;$$

$$U_a(\theta) = \sum_{n=0}^{7}\int_{(n-1)\Lambda+b}^{n\Lambda} E_{a_n}(x,n)\xi(x,\theta)dx;$$

$$U_4(\theta) = \int_{n\Lambda}^{\infty} E_4(x)\xi(x,\theta)dx;\ \xi(x,\theta) = \exp(ik_0x\sin\theta).$$

Parameter $U_i(0)$ is determined by the same relations at $\theta = 0$.

In our numerical simulation of a one-dimensional multilayer waveguide, we will seek the active waveguide thickness satisfying a beam divergence of 30° and the corresponding optical confinement factor. The larger the optical confinement factor, the lower the threshold pump current density [17]:

$$J_{th} = \frac{ed}{\tau_n}n_{th} = \frac{ed}{\tau_n}\left(n_0 + \frac{1}{c\tau_p g_0 \Gamma_{ac}}\right), \quad (12)$$

where e is the electron charge; d is the active region thickness; τ_n is the lifetime of carriers; n_{th} is the threshold carrier density; g_0 is the differential gain; c is the velocity of light in the material; n_0 is the carrier density at which the material is bleached; and τ_p is the photon lifetime in the cavity.

To analyse the effect of the geometry of a multilayer optically coupled waveguide on the divergence and the optical confinement factor, we use the HS schematically shown in Fig. 1. The structure with one active waveguide and several passive waveguides ($N = 7$) is used as basic.

3. Calculation results and discussion

3.1. Choice of the active waveguide thickness

The optical confinement factor and divergence depend on the active waveguide thickness and the AR positon on this wave-

guide. The electric field distribution, as well as dependences of the optical confinement factor Γ_{ac} and the divergence angle of the zero and first modes will be analysed at active waveguide thicknesses of 0.04, 0.414, and 1.24 μm. Figure 2 presents the dependences of factor Γ_{ac} and divergence angle θ of the zero mode on the active waveguide thickness L_w. One can see that a decrease in L_w leads to a decrease in both Γ_{ac} and θ, while an increase in L_w increases θ and almost does not change Γ_{ac}.

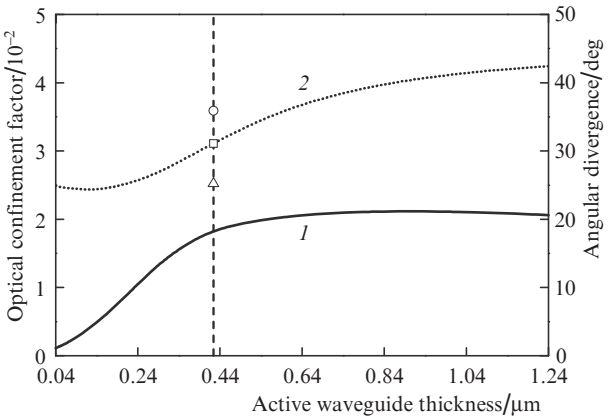

Figure 2. Dependences of (*1*) optical confinement factor Γ_{ac} and (*2*) angular divergence θ for the zero mode on the active waveguide thickness L_w. The vertical line indicates thickness L_w = 0.424 μm. Experimental points ○, △ and □ correspond to the maximum, minimum, and average θ from [6].

To choose the optimal, in our opinion, active waveguide thickness, we will analyse the behaviour of Γ_{ac} and θ at three characteristic points of dependences in Fig. 2. Figure 3a shows the distributions of the refractive index and electric field of the zero and first modes, while Fig. 3b shows the far-field intensity distribution for the zero and first modes at the active waveguide thickness of 0.04 μm ($L_1 = L_2 = 0.013$ μm). One can see that the electric field of the first mode maximally overlaps with the periodic layers. This field distribution indicates an increase in the volume occupied by the field and, as a result, a decrease in the radiation divergence. At the same time, the overlap of the electric field with the active region is minimal, which leads to low optical confinement factors. Thus, we have $\Gamma_{ac} = 0.00116$ and $\theta = 24.9°$ for the zero mode and $\Gamma_{ac} = 0.00387$ and a two-lobe radiation pattern for the first-order mode (Fig. 3b). It is clear that the choice of this active waveguide thickness is unreasonable.

The same dependences for the zero and first modes for the active waveguide thickness of 0.414 μm ($L_1 = L_2 = 0.2$ μm) are shown in Figs 3c and 3d. In this case, the zero mode field is less overlapped with the periodic layers than in the previous case. However, the optical field maximum almost coincides with the active region, which leads to an increase in the optical confinement factor and divergence, namely to $\Gamma_{ac} = 0.01758$ and $\theta = 30.56°$ for the zero mode and to $\Gamma_{ac} = 0.00242$ and $\theta = 47.2°$ for the first mode. Analysis shows that only the zero mode will be excited in this case, because its optical confinement factor is almost an order of magnitude higher than that of the first mode.

Finally, Figs 3e and 3f show the same dependences for the active waveguide thickness 1.24 μm ($L_1 = L_2 = 0.613$ μm). One can see that the optical field of the zero mode in this case decays faster than in the previous case and weaker overlaps with the periodic optically coupled waveguide. The electric field maximum in this case well coincides with the active region, which leads to a higher optical confinement factor than that in the case of the active waveguide thickness 0.414 μm. We have $\Gamma_{ac} = 0.0208$ and $\theta = 42.46°$ for the zero mode and $\Gamma_{ac} = 0.00041$ and $\theta = 33.5°$ for the first-order mode. As in the previous case, only the zero mode will be excited, since its optical confinement factor is 50 times higher than that of the first mode.

The electric field distributions of the zero and first modes presented in Figs 3c and 3e are similar to the distributions presented in Fig. 2 of work [5].

Thus, the active waveguide thickness 0.414 μm meets the requirement of a ~30° radiation divergence. However, the

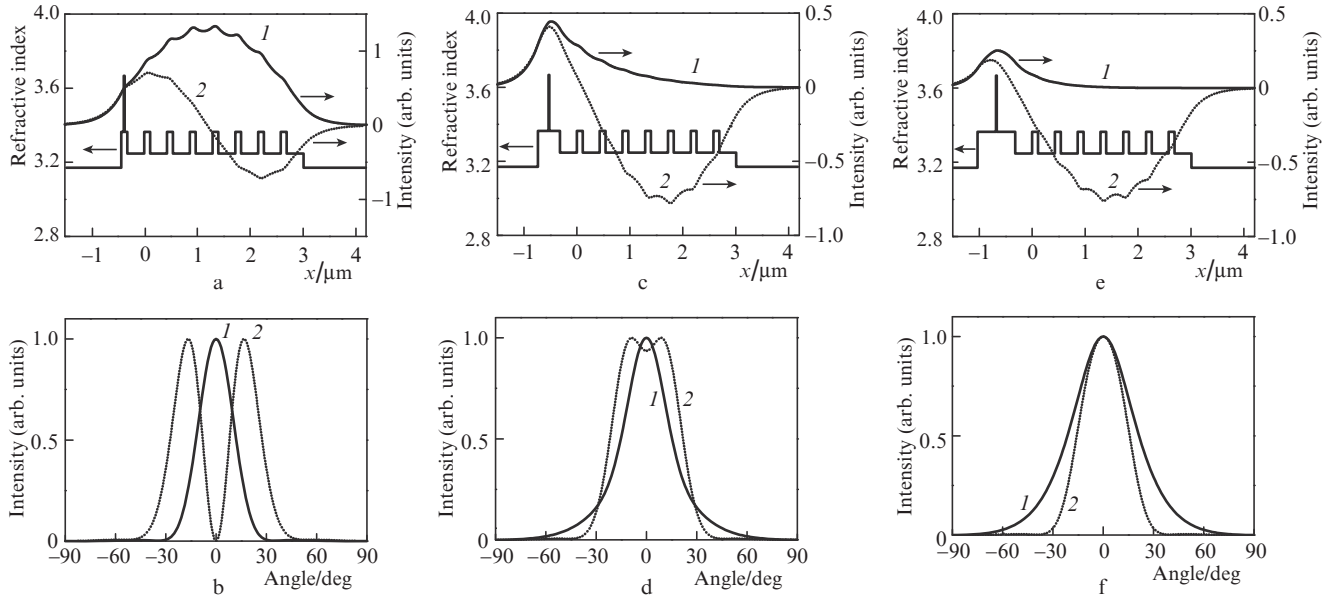

Figure 3. (a, c, e) Distributions of the refractive index and the electric field of the (*1*) zero and (*2*) first-order modes, as well as (b, d, f) far-field intensity distributions for the (*1*) zero and (*2*) first-order modes at active waveguide thicknesses of (a, b) 0.04, (c, d) 0.414 μm, and (e, f) 1.24 μm.

active waveguide thickness 1.24 μm is the best choice for improving the power and threshold characteristics of lasers without taking divergence into account.

3.2. Choice of the optimal active region position on the waveguide

Let us consider the case of the AR position at the right edge of the active waveguide ($L_1 = 0$, $L_2 = 0.4$ μm), when $\Gamma_{ac} = 0.01545$ and $\theta = 30.8°$, and the case of the AR position at the left edge of the waveguide ($L_1 = 0.4$ μm, $L_2 = 0$), when $\Gamma_{ac} = 0.00827$ and $\theta = 29.11°$. Therefore, the optical confinement factors in the first and second cases are, respectively, 1.14 and 2.13 times lower than in the case of $L_1 = L_2 = 0.2$ μm with almost the same radiation divergence. Analysis of the results presented in Fig. 3 show that the optimal position of the active region on the waveguide corresponds to the position of the maximum of the zero mode electric field distribution. At $L_1 = 0.16$ μm and $L_2 = 0.24$ μm, the parameters $\Gamma_{ac} = 0.01819$ and $\theta = 30.17°$ for the zero mode are better than at $L_1 = L_2 = 0.2$ μm. The recommended active waveguide thickness is 0.424 μm with $L_1 = 0.17$ μm and $L_2 = 0.24$ μm; in this case, for the zero mode we have $\Gamma_{ac} = 0.01859$ and $\theta = 31.42°$. Thus, an increase in Γ_{ac} leads to an increase in θ.

The active waveguide thickness recommended for growing is indicated in Fig. 2 by the vertical line. The central point on this line corresponds to the average divergence, and the other two points indicate the spread of experimental values of radiation divergence obtained in [6].

3.3. Choice of the optimal grating parameters

Figure 4 presents the dependences of the optical confinement factor and angular dispersion on the grating period. The vertical line indicates the grating period recommended in [6] for growing a HS with $N = 7$, which corresponds to calculated parameters $\theta = 31.42°$ and $\Gamma_{ac} = 0.01859$. Increasing the grating period by a factor of 2.5 (to $\Lambda = 1.075$ μm), it is possible to decrease the angular divergence to 15.9° (almost twofold) and decrease the optical confinement factor by 19%. However, this was not done in [6] because the thickness of seven layers in this case would be 7.525 μm, which could lead to an increase in the voltage drop across the HS and its thermal resistance and, hence, to deterioration of the power characteristics of the laser due to its additional heating. The experimental points in Fig. 4 correspond to the maximum, minimum, and average values of θ from [6]. Thus, we can conclude that the recommended grating period is $\Lambda = 0.43$ μm.

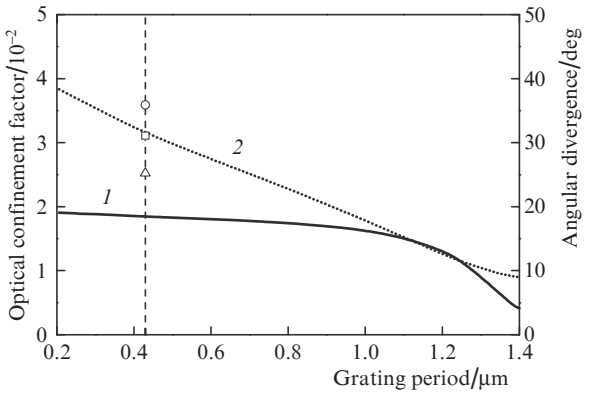

Figure 4. Dependences of (*1*) optical confinement factor Γ_{ac} and (*2*) angular divergence θ for the zero mode on the grating period Λ. The vertical line indicates period $\Lambda = 0.43$ μm. Experimental points ○, △ and □ correspond to the maximum, minimum, and average θ from [6].

Calculations of the dependences of the optical confinement factor and divergence on the thickness b of the grating layer with a high refractive index show that it is reasonable to choose $b = 0.11$ μm. It makes no sense to increase the layer thickness b (retaining the grating period) because the optical confinement factor in this case decreases while the radiation divergence almost does not change. It is also useless to decrease thickness b below 0.11 μm, because this simultaneously increases the optical confinement factor and the divergence. Thus, the recommended layer thickness is $b = 0.11$ μm.

Figure 5 presents the experimental and theoretical far-field intensity distributions at a cw laser power of 100 mW. One can see that the experimentally measured divergence well coincides with the distribution calculated by formula (11).

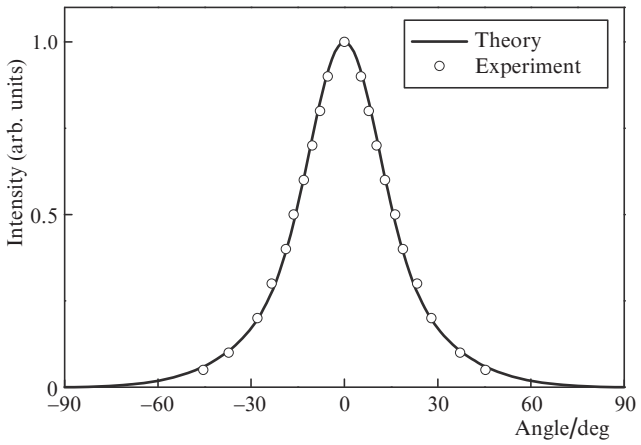

Figure 5. Experimental and theoretical far-field radiation intensity distributions at a laser power of 100 mW.

Let us now consider a grating with the number of layers $N = 4$ and a period increased by a factor of 2.5. According to calculations, this increase will lead to a twofold decrease in the beam divergence and to a decrease in the optical confinement factor by 2.5 times rather than by 19% as is was at $N = 7$. Therefore, for a grating with $N = 4$, it is unreasonable to decrease the radiation divergence by increasing the grating period.

References

1. Gorlachuk P.V., Ivanov A.V., Kurnosov V.D., Kurnosov K.V., et al. *Quantum Electron.*, **48**, 495 (2018) [*Kvantovaya Elektron.*, **48**, 495 (2018)].
2. Bagaeva O.O., Danilov A.I., Ivanov A.V., Kurnosov K.V., et. al. *Quantum Electron.*, **49**, 649 (2019) [*Kvantovaya Elektron*, **49**, 649 (2019)].
3. Ledentsov N.N., Shchukin V.A. *SPIE Opt. Eng.*, **41**, 3193 (2002).
4. Maximov M.V., Shemyakov Y.M., Novikov I.I., et al. *Proc. SPIE*, **6115**, 611513 (2006).
5. Liu L., Qu H., Liu Y., Zhang Y., et al. *Appl. Phys. Lett.*, **105**, 231110 (2014).
6. Bagaeva O.O., Danilov A.I., Ivanov A.V., et. al. *Quantum Electron.*, **50**, 600 (2020) [*Kvantovaya Elektron.*, **50**, 600 (2020)].
7. Ivanov A.V., Kurnosov V.D., Kurnosov K.V., Marmalyuk A.A., Romantsevich V.I., et al. *Quantum Electron.*, **37**, 545 (2007) [*Kvantovaya Elektron.*, **37**, 545 (2007)].

8. Yeh P., Yariv A., Hong C.S. *J. Opt. Soc. Am.*, **67**, 423 (1997).
9. Yariv A., Yeh P. *Optical Waves in Crystals* (New York: Wiley, 1984).
10. Yariv A., Yeh P. *Photonics: Optical Electronics in Modern Communications* (New York: Oxford, 2007).
11. Shiraz H.G. *Distributed Feedback Laser Diodes and Optical Tunable Filters* (Wiley and Sons Ltd, 2003).
12. Anemogiannis E., Glytsis E.N., Gaylord T.K. *Ligtwave Technol.*, **12**, 2080 (1994).
13. Chilwell J., Hodkinson I. *J. Opt. Soc. Am. A*, **1**, 742 (1984).
14. Yariv A. *Introduction to Optical Electronics* (New York: Holt, Rinehart and Winston, 1976).
15. Eliseev P.G. *Vvedenie v fiziku inzhektsionnykh laserov* (Introduction to Physics of Injection Lasers) (Moscow: Nauka, 1983).
16. Casey H.C., Panish M.B. *Heterostructure Lasers* (New York: Academic Press, 1978).
17. Numai T. *Fundamentals of Semiconductor Lasers* (Springer, 2004).